International Journal of Refrigeration 169 (2025) 152–165

Contents lists available at ScienceDirect

International Journal of Refrigeration

journal homepage: www.elsevier.com/locate/ijrefrig

INSTITUT INTERNATIONAL DU FROID
INTERNATIONAL INSTITUTE OF REFRIGERATION

High-fidelity model development of CO_2 booster refrigeration systems in supermarkets using field measurements

Développement d'un modèle haute fidélité de systèmes de réfrigération booster de CO2 dans les supermarchés à l'aide de mesures sur le terrain

Wenzhuo Li, Ivan Korolija, Rui Tang *, Dejan Mumovic

Institute for Environmental Design and Engineering, The Bartlett, University College London, UK

ARTICLE INFO

Keywords:
Food retail store
R744 refrigeration systems
Theoretical model
Heat recovery
Energy decarbonization

Mots-clés:
Magasin de détail alimentaire
Systèmes de réfrigération r744
Modèle théorique
Récupération de chaleur
Décarbonisation énergétique

ABSTRACT

Supermarket refrigeration systems adopting traditional refrigerants with high global warming potential (GWP) have impacts on global warming for indirect and direct greenhouse gases (GHG) emissions. CO_2 is a popular low-GWP alternative. The transcritical operation of CO_2 systems worsens their energy performance, but provides recoverable heat as a heat source to reduce gas consumption. To evaluate operation performance, data-driven models, trained by historical data, are weak in implementation with datasets outside the scope of training data; in contrast, theoretical models have better extrapolation ability to calculate all operation conditions of CO_2 systems at supermarket. Existing theoretical modeling approaches often lack validation against the limited public-access data, which reduces model reliability for further applications, and adopt oversimplified inference methods for unmeasured variables, which increases the risks of breaking thermodynamic laws and lowering model accuracy. This study therefore develops a steady-state theoretical model for CO_2 booster refrigeration systems validated against field measurements from three UK supermarkets. The available measurements are utilized to the best level to ensure model accuracy and physical interpretability. Proposed methods to infer missing variables in CO_2 systems include condenser outlet temperature, evaporating temperature, compressor isentropic efficiency and compressor mass flow rate. Results show that proposed inference methods enhance the abilities of the proposed modeling approach to ensure data integrity, avoid breaking thermodynamic laws, and improve model accuracy by reflecting real-time actual values of unmeasured variables rather than rough assumptions. The proposed modeling approach provides satisfactory accuracy validated using high-resolution measurements across the whole year from three real supermarkets.

1. Introduction

Supermarkets, a typical type of food retail buildings, are featured with high energy intensity to maintain customer comfort and food freshness (Gulliford et al., 2022). Based on the European Union (EU) Building Stock Observatory (European Commision 2024), it shows that about 23 % of the final energy used in European non-residential buildings corresponds to wholesale and commercial retail trade operations (Royal Institution of Chartered Surveyors (RICS) 2020). According to the Building Energy Efficiency Survey (BEES) (Department for Business 2024) carried out in England and Wales, the retail sector consumes more than 17 % of the total non-domestic building stock energy. Among multiple supermarkets' electricity end users, about 35–60 % of the supermarkets' electricity consumption is associated with refrigeration systems (Mylona et al., 2017; Lagoeiro et al., 2024). Therefore, there is a great potential for energy efficiency improvement in the refrigeration systems of supermarkets.

The retail industry is one of the top-ranked carbon-intensive business sectors (Ferreira et al., 2019). Based on goods sold, about 62 % of the annual UK retail greenhouse gases (GHG) emissions which is the largest share comes from the food, drinks and tobacco retailers (British Retail Consortium (BRC) 2024). In supermarkets, there are indirect GHG emissions owing to the high electricity usage as well as direct GHG emissions owing to the leakage of refrigerant with high global warming potential (GWP) (Hart et al., 2020; Maouris et al., 2020). The

* Corresponding author.
E-mail address: rui.tang@ucl.ac.uk (R. Tang).

https://doi.org/10.1016/j.ijrefrig.2024.10.025
Received 10 July 2024; Received in revised form 16 October 2024; Accepted 20 October 2024
Available online 21 October 2024

Nomenclature

a1-a10	Coefficients for isentropic efficiency
b1-b10	Coefficients for mass flow rate estimation
cf	Correction factor
h	Specific enthalpy
m	Mass flow rate
AHU	Air-handling unit
BMS	Building management system
GHG	Greenhouse gases
GWP	Global warming potential
HFC	Hydrofluorocarbon
HP	High-pressure
HP%	Capacity of HP compressor
LP	Low-pressure
LP%	Capacity of LP compressor
LT	Low temperature
M1-M8	The 1st to 8th models
MT	Medium temperature
N	Number
P	Pressure
Q	Heat transfer rate
R	Ratio
S1, S2	The 1st and 2nd refrigeration systems
SH	Superheat
T	Temperature
VSD	Variable speed drive
W	Power

Greek symbols

η	Isentropic efficiency
τ	Compression ratio

Subscripts and superscripts

me	Mechanical
min	Minimum
multi	Multiple variable fitted
on/off	On/off controlled compressor
sat@(T_{Amb}+3)	Saturated pressure at T_{Amb}+3
sub/trans	Subcritical or transcritical mode
Amb	Ambient
AV	Air volume
Cal	Calculated
Crit	Critical
GC	Gas cooler
HP	High-pressure compressor
LP	Low-pressure compressor
LT	Low temperature evaporator
MT	Medium temperature evaporator
Tot	Total
VSD	VSD compressor
1–16	States 1–16
τ	Compression ratio fitted

refrigerants predominantly used in the UK supermarket refrigeration systems are hydrofluorocarbon (HFC) refrigerants (e.g. R404A), which are high-GWP refrigerants (Salehy et al., 2020). It is estimated that the average refrigerant emission rate of refrigeration systems in the United States was about 12.9 % in 2021 (The GreenChill Program 2022) and the annual CO_2 equivalent emissions of the refrigerant leakage in European countries were about 148 million tons (Mota-Babiloni et al., 2015) (Paurine et al., 2021). Therefore, the replacement of high-GWP refrigerants is critical and the natural working fluids with low GWP are promising alternatives to reduce direct GHG emissions (Sun et al., 2020).

CO_2 (R744), a natural refrigerant with very low GWP, has received growing attention to be used in supermarket refrigeration systems. Around 30 % increase per year of CO_2 refrigeration systems installation in supermarkets was observed between 2013 and 2016 (Skačanová, 2016). The standard CO_2 booster refrigeration systems are popular for their simpler and cheaper system designs (Ge and Tassou, 2011). However, standard CO_2 refrigeration systems are likely to have worse energy performance when compared to HFC/HCFC refrigeration systems considering the comparably high operating pressure and low critical temperature of CO_2 (Polzot et al., 2017). Specifically, to ensure the heat transfer between CO_2 refrigerant and the outdoor air when the ambient temperature is high (e.g. summer), CO_2 refrigeration systems would operate under the transcritical mode with high discharge pressure of compressors (Sacasas et al., 2022). This leads to increased electricity consumption and decreased Coefficient of Performance (COP) of CO_2 refrigeration systems (D'Agaro et al., 2019). However, the transcritical operation mode is also featured with the high discharge temperature of compressors, which provides great opportunities for heat recovery (Tsamos et al., 2017). Specifically, through heat exchangers or de-superheaters, the recoverable heat can be used for heating demand provision to reduce the gas consumption for heating system decarbonization. On the other hand, various technical solutions have been investigated for the CO_2 refrigeration systems to achieve better performance compared to the standard CO_2 systems and comparable performance compared to the traditional HFC systems, such as the CO_2 partial cascaded two-stage compression refrigeration system (Sun et al., 2020) and the integrated CO_2 refrigeration system with multi-ejectors (Söylemez et al., 2022). Therefore, CO_2 refrigeration systems are a promising measure to tackle climate change.

CO_2 booster refrigeration systems and heat recovery implementations are increasingly investigated. Maouris et al. (2020) investigated the performance of a CO_2 booster system integrated with thermal storage. The CO_2 booster system was responsible for meeting space heating demand and the cooling demand of chilled and frozen food cabinets. A thermal storage system was responsible for storing the recoverable heat which exceeded the heating demand during certain periods. Azzolin et al. (2021) analyzed the field measurements from CO_2 booster refrigeration systems at an Italian supermarket. It was found that the heating demand was completely satisfied using heat recovery by driving the CO_2 systems to transcritical conditions and activating the external evaporator. Sawalha (2013) analyzed the cooling and heating COPs of the CO_2 transcritical refrigeration system at different ambient temperatures for floating condensing and heat recovery modes. In relatively cold climates, CO_2 booster refrigeration systems were found to be more efficient in simultaneous cooling and heating provision than conventional refrigeration systems with heat pumps as separate heat sources. To cover a full heating load, i.e. domestic hot water (DHW) and space heating, Polzot et al. (2016) assessed the performance of an additional air-cooled load evaporator in CO_2 booster systems to increase the recoverable heat. System performances are analyzed based on the developed models. Data-driven models are trained by historical data which is hard to cover all the operation conditions. Typically, the historical data of CO_2 booster refrigeration systems are collected from the floating condensing operation condition, but there are other operation conditions of interest where the datasets are extremely apart from historical datasets, such as different heat recovery operation conditions. Given this, the developed data-driven models cannot be extrapolated to test different heat recovery strategies (Liang et al., 2023). In contrast, theoretical models work well in both the interpolation scenario, i.e. floating condensing

operation condition, and the extrapolation scenario, i.e. heat recovery operation conditions.

Theoretical modeling is widely used in evaluating the performance of CO_2 refrigeration systems. Sarabia Escriva et al. (2019) developed a steady-state model for a CO_2 booster system. The model accuracy was regarded as satisfactory as the mean average percentage error was 11 %, the annual energy error was 0.12 % and the coefficient of determination (R^2) was 0.86. Maouris et al. (2020) further integrated a one-dimensional thermal storage model with this CO_2 booster system model. Sarabia Escriva et al. (2022) integrated a zero-dimensional thermal storage model with this CO_2 booster system model. Both works assessed different configurations and operation strategies for both space heating and food preservation in a UK supermarket by conducting techno-economic analysis. Liu et al. (2019) established the theoretical model for a newly proposed transcritical CO_2 refrigeration cycle integrated with thermoelectric subcooler and ejector based on mass, momentum, and energy conservation. It was then used to do comparisons with the conventional transcritical CO_2 refrigeration cycle (BASE), CO_2 cycle with a thermoelectric subcooler (TES) and CO_2 cycle with an ejector (EJE). Liu et al. (2020) analyzed the theoretical model for a novel two-stage compression transcritical CO_2 dual-evaporator refrigeration cycle with an ejector thermodynamically to show its better than those of conventional system. However, most of the models were not validated against the field measurements to show their accuracy. For those limited number of works with model validation process (e.g. (Sarabia Escriva et al., 2019)) the deviation between the modeled and actual values was relatively high. Furthermore, one of the main challenges for developing theoretical models using real data is the limited availability of data needed in model development. These works either adopted simplified inference methods for unavailable variables (e.g. by assuming a constant) or explained vaguely or even omitted the inference methods. As a summary, conventional theoretical modeling approaches lack a validation process against the limited public-access data, which reduces the reliability of the developed model for further applications, and adopt an oversimplified inference method for unavailable variables, which increases the risk of the developed model breaking thermodynamic laws and deteriorating modeling performance.

This study therefore develops a steady-state theoretical model for CO_2 booster refrigeration systems validated against field measurements from three UK supermarkets. The available measurements are utilized to the best level to ensure the model accuracy and physical interpretability. Methods to infer the missing information in CO_2 refrigeration systems are proposed. This study has three major contributions. (1). Inference methods for missing variables that are normally unavailable in the field measurements but critical in model development are proposed by fully utilizing the actual operation datasets from the Building Management System (BMS) of three UK stores and the compressor performance datasets from the manufacturer. They are condenser outlet temperature, evaporating temperature, compressor isentropic efficiency and compressor mass flow rate. (2). Proposed inference methods for missing variables ensure data integrity and avoid breaking thermodynamic laws. This is of vital importance when new operation settings (e.g. heat recovery strategies) are tested by developed models before being put into practice. (3). The proposed model approach provides satisfactory model accuracy by the validation process using high-resolution field measurements across the whole year from the CO_2 booster refrigeration systems in three real UK supermarkets.

2. Model development of CO_2 booster refrigeration systems

This section first describes the operation of a standard CO_2 booster refrigeration system. The theoretical model is elaborated through the main equations describing the thermodynamic cycle. In these equations, the variables normally available from field measurements are explained. The rest missing variables unavailable from field measurements are estimated using the proposed methods.

2.1. System description

The schematic of a standard CO_2 booster refrigeration system is shown in Fig. 1. The pressure-enthalpy diagrams representing the CO_2 booster refrigeration cycles are shown in Fig. 2. The main tasks of CO_2 booster refrigeration systems are to maintain the frozen (cold rooms and freezers) and chilled (fridges and display cabinets) food cabinets at preset temperatures using the low temperature (LT) and medium temperature (MT) evaporators respectively. The superheated vapor from the LT evaporators (state 1) is boosted by the low-pressure (LP) compressors to the MT level (state 2), which is the term "booster" refers to (Giunta and Sawalha, 2021). It is further compressed by the high-pressure (HP) compressors after mixing with the refrigerant from the MT evaporators (state 14) and the flash tank (state 10). The refrigerant at the outlet of HP compressors (state 5) is in a high-temperature state. To reduce the discharge temperature, the heat will be rejected in the condenser (subcritical cycle)/the gas-cooler (transcritical cycle) in this standard booster CO_2 system. The flash tank is used to separate the gas-liquid mixture of refrigerant into liquid (state 11) and gas (state 9) at an intermediate pressure. The liquid is distributed to the MT and LT evaporators, while the flash gas goes to the suction of the HP compressors. As one of the popular decarbonization strategies following the Paris Agreement to tackle climate change (Granell et al., 2021), heat recovered from a booster CO_2 system by installing an additional heat exchanger between the HP compressor and the gas cooler/condenser of a standard CO_2 booster refrigeration system, as shown in the dashed box of Fig. 1, can be transferred to the water circuit and linked to an air-handling unit (AHU) to be used as another heating source to suppress natural gas consumption. This work mainly focuses on model development for standard CO2 booster refrigeration systems, thus heat exchangers and heat recovery are not considered here but are investigated in the follow-up studies.

2.2. Model description

The steady-state theoretical model developed in this study is based on the main equations describing the thermodynamic cycle of CO_2 booster refrigeration systems, as presented in Eqs. (1)–(9). The variables with a number in subscript correspond to the properties at certain states numbered in Figs. 1 and 2. The total electric power of individual CO_2 booster refrigeration system ($W_{Tot,Cal}$) is shown in Eq. (1). The LP and HP compressors' power (W_{LP} and W_{HP}, kW) are calculated using Eqs. (2) and (3). m_{LP} and m_{HP} are the refrigerant mass flow rates of LP and HP compressors (kg s^{-1}). h_5 and h_4 are the specific enthalpies of refrigerant at the outlet and inlet of HP compressors (kJ/kg). $\eta_{me,LP}$ and $\eta_{me,HP}$ are

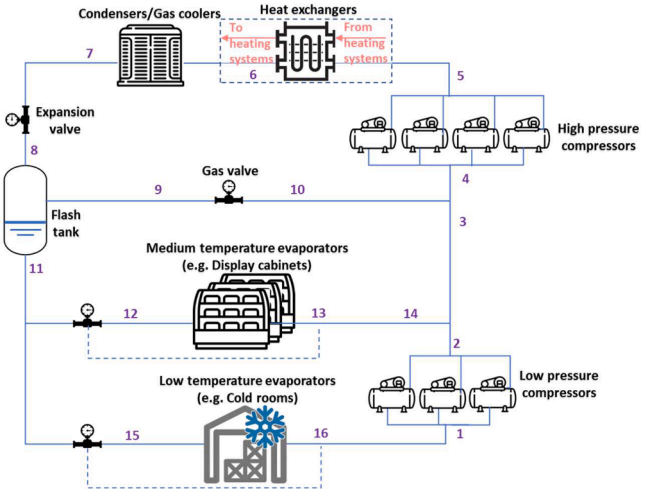

Fig. 1. Schematic of a standard CO_2 booster refrigeration system.

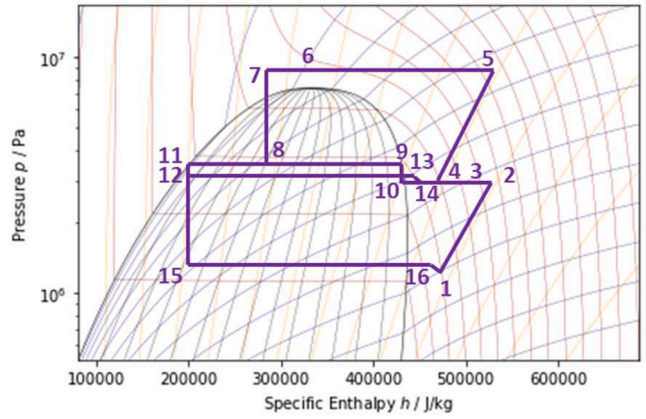

Fig. 2. Representations of CO_2 booster refrigeration cycle in the pressure-enthalpy diagram.

the mechanical efficiencies of LP and HP compressors, $\eta_{me,LP} = 0.90$ and $\eta_{me,HP} = 0.90$. The gas cooler/condenser fan power (W_{Fan}, kW) is calculated using Eq. (4) (The GreenChill Program 2018). R_{AV} is the air volume ratio, calculated by Eq. (5). $Q_{GC,rated}$ is the rated heat rejection rate in gas coolers/condensers (kW). $W_{Fan,design}$ is the gas cooler/condenser fan power under the designed condition (kW).

$$W_{Tot,Cal} = W_{LP} + W_{HP} + W_{fan} \tag{1}$$

$$W_{LP} = \frac{m_{HP}(h_2 - h_1)}{\eta_{me,LP}} \tag{2}$$

$$W_{HP} = \frac{m_{HP}(h_5 - h_4)}{\eta_{me,HP}} \tag{3}$$

$$W_{fan} = {R_{AV}}^{2.5} W_{fan,design} \tag{4}$$

$$R_{AV} = \left(\frac{Q_{GC}}{Q_{GC,rated}}\right)^{\frac{1}{0.633}} \tag{5}$$

For LT and MT evaporators, the cooling capacities (Q_{LT} and Q_{MT}, kW) are calculated using Eqs. (6) and (7). h_{16} and h_{15} are the specific enthalpies of refrigerant at the outlet and inlet of LT evaporators (kJ/kg). h_{13} and h_{12} are the specific enthalpies of refrigerant at the outlet and inlet of MT evaporators (kJ/kg). m_{MT} is the refrigerant mass flow rate of MT evaporators (kg s^{-1}). The refrigerant mass balance is shown as Eq. (8). m_9 is the bypass refrigerant mass flow rate which leaves the flash tank (kg s^{-1}).

$$Q_{LT} = m_{LP}(h_{16} - h_{15}) \tag{6}$$

$$Q_{MT} = m_{MT}(h_{13} - h_{12}) \tag{7}$$

$$m_{HP} = m_{MT} + m_{LP} + m_9 \tag{8}$$

The heat rejection rate in gas coolers/condensers (Q_{GC}, kW) is shown in Eq. (9). h_5 and h_7 are the specific enthalpies of refrigerant at the inlet and outlet of the gas cooler/condenser (kJ/kg).

$$Q_{GC} = m_{HP} \cdot (h_5 - h_7) \tag{9}$$

Based on Eqs. (1)–(9), the model is developed with the model inputs of the discharge pressure of HP (P_5) and LP compressors (P_2), the real-time capacities of individual HP (*HP%*) and LP (*LP%*) compressors and the ambient temperature (T_{Amb}). The model output is the total electric power of individual CO_2 booster refrigeration systems ($W_{Tot,Cal}$), including compressors and gas cooler fans. For variables in Eqs. (1)–(9), some of them are available from field measurements which is illustrated in Section 2.3, while others need to be estimated carefully which is illustrated in Section 2.4.

2.3. Field measurements for the model development

The enthalpy terms in Eqs. (1)–(9) are calculated based on the temperatures and pressures which are directly measured in the system or indirectly estimated according to the design documents (Inderwildi et al., 2020). Normally, the discharge pressure of HP ($P_5 = P_6 = P_7$) and LP ($P_2 = P_4 = P_{10} = P_{14}$) compressors, and the ambient temperature (T_{Amb}) are directly monitored in the system. By referring to the as fitted drawings and engineering sheets of the store, the evaporating temperature in MT (T_{12}) and LT (T_{15}) evaporators, the designed condenser/gas cooler approach temperature (min(T_7-T_{Amb})), the suction gas superheat (T_{14}-$T_{13} = T_1$-T_{16}), the useful superheat (T_{13}-$T_{12} = T_{16}$-T_{15}) and the flash tank pressure ($P_8 = P_9 = P_{11}$) and the suction line pressure drop (P_{12}-$P_{14} = P_{15}$-P_1) are obtained. Here, the approach temperature is the smallest temperature difference between CO_2 refrigerant at the outlet of the condenser/gas cooler and the ambient air. The suction gas superheat is also called the non-useful superheat, which is due to the long distance between LP and HP compressors (located in the machine room on the roof of the supermarket) and LT and MT evaporators (located in the shopping area of the supermarket). The useful superheat is in the refrigerated space, which contributes to the cooling capacity and thus is useful. It is worth noting that the suction line pressure drop, which is due to the long refrigerant distribution pipes, is sometimes shown with the temperature unit (e.g. 2 °C) in design documents. This is because it is equivalently represented as saturation temperature decrease. For example, the saturation temperature at P_{12} and P_{15} are 2 °C higher than at P_1 and P_4.

The real-time capacities of individual HP (*HP%*) and LP (*LP%*) compressors are another set of variables, which are critical in model development and directly measured in the system. They impact the mass flow rate terms in Eqs. (1)–(9). To match the changing cooling load of MT evaporators, HP compressors operate with different capacities by different control modes. Specifically, the variable speed drive (VSD) controlled compressors adjust their speeds while the on/off controlled compressors switch on/off accordingly when necessary. To match the changing cooling load of LT evaporators, LP compressors are usually on/off controlled.

The energy data are normally measured in the system. The measured electricity consumption, including compressors and gas cooler fans, of individual CO_2 booster refrigeration systems is critical in model development since it will be compared with the model output for model validation.

2.4. Methods of inferring missing variables in the model development

Though most variables are not difficult to obtain nowadays, it only works in experimental conditions or pilot projects as small-scale

industrial applications. Our work is intended for CO_2 systems in large-scale industrial applications, in which store owners and managers are reluctant to install additional sensors in practice, instead they prefer to follow the conventional sensor installation plans. Therefore, considering the limited available data from conventional sensor installation plans, those unavailable variables need to be estimated for model development, including condenser/gas cooler outlet temperature, evaporating temperature, compressor isentropic efficiency and compressor mass flow rate. Besides the actual system operation data from BMS, compressor performance data from the manufacturer is another type of dataset utilized in this study. They are used in the proposed inference methods of this study. It is worth noting that evaporating temperature is given in store design documents, but sometimes it is contradictory to another measured variable. This section investigates different methods, i.e. the conventional methods and the proposed methods in this study, to infer missing variables for data integrity.

2.4.1. Condenser/Gas cooler outlet temperature

The gas cooler acts as a condenser to reduce the discharge temperature of HP compressors through a single-phase gas cooling process without liquid condensation under the transcritical mode (Polzot, 2017). Therefore, although condenser and gas-cooler are the same device, the terms are used in subcritical and transcritical modes separately in this study.

The condenser outlet temperature under the subcritical mode is the saturated temperature at the discharge pressure of HP compressors (P_5). It should be no smaller than the ambient air temperature plus the approach temperature, as mentioned in Section 2.3. However, some abnormal circumstances were identified after the preliminary data analysis that the condenser outlet temperature (under the subcritical mode) is higher than the ambient air temperature but lower than the ambient air temperature plus the designed approach temperature. There are also some cases where the condenser outlet temperature is smaller than the ambient air temperature which is thermodynamically impossible. These abnormal circumstances were expected to result from incorrect sensor readings. Therefore, two schemes, i.e. (a) and (b), on estimating condenser outlet temperature under the subcritical mode are tested to eliminate these abnormal data, as listed in Table 1. Scheme (a) is recommended by the store design documents that if the temperature difference between the condenser outlet temperature (T_7) and the ambient temperature (T_{Amb}) is less than the approach temperature, T_7 is set as T_{Amb} plus the approach temperature. Scheme (b) is proposed in this work for correcting the wrongly measured discharge pressure of HP compressors (P_5), as shown in Fig. 3. The idea is to increase P_5, which is expected to be wrongly read thus breaking the thermodynamic laws, to a new value (P_{5new}) depending on how close the operating condition is to the critical point. Specifically, if the temperature difference between the critical temperature (T_{Crit}) and T_{Amb} is <3 °C, P_{5new} is reset as the saturated pressure at $T_{Amb} + 3$ ($P_{sat@(TAmb+3)}$). Otherwise, P_{5new} is reset as a transcritical pressure by assuming a constant entropy at the condenser outlet ($s_7 = s_{7new}$), unless this results in unrealistically large discharge pressures in which cases the P_{5new} is fixed to 75 Bar.

On the other hand, the gas cooler outlet temperature (T_7) (under the transcritical mode) is set to be 3 °C higher than the ambient temperature (T_{Amb}) according to the store design documents.

2.4.2. Evaporating temperature

The evaporating temperature in MT (T_{12}) and LT (T_{15}) evaporators obtained from the store design documents are usually adopted in model development by assuming that the pressure as well as evaporating temperature in MT and LT evaporators are constant across the year. The discharge pressure of LP compressors (P_2) is also constant across the year by assuming a constant suction line pressure drop. This results in the inability to utilize the actual measured P_2 changing with the real-time system operation across the year. In contrast, the evaporating temperature (T_{12}) in MT evaporators can also be calculated by using available variables from field measurement including the discharge pressure of LP compressors ($P_2 = P_{14}$) and the suction line pressure drop (P_{12}-P_{14}). Therefore, two schemes on evaporating temperature in MT evaporators, i.e. to be a constant as the conventional method and to be variable calculated from field measurements as the proposed method, are tested in model development, as listed in Table 1. On the other hand, the evaporating temperature in LT evaporators is still assumed constant across the year considering the good insulation of cold rooms and freezers (LT evaporators).

2.4.3. Compressor isentropic efficiency

Compressor isentropic efficiency (η_i) (Pérez-Segarra et al., 2005) is a critical variable needed in model development but is usually not provided in the store design documents. Therefore, two schemes, i.e. single variable fitted isentropic efficiency as the conventional method and multiple variables fitted isentropic efficiency as the proposed method, on estimating compressor isentropic efficiency are tested in model development, as listed in Table 1.

The conventional method fits isentropic efficiency for LP and HP compressors ($\eta_{i,LP,\tau}$ and $\eta_{i,HP,\tau}$) as functions of the compression ratio (τ_{LP} and τ_{HP}) between the discharge and suction pressures of LP and HP compressor (Sarabia Escriva et al., 2019; Polzot, 2017; Gullo et al., 2016), shown as Eqs. (10) and (11). The data from the compressor manufacturer (Bitzer) are used for fitting using the curve fitting tool in MATLAB. Fig. 4 shows the manufacturer data of LP and HP compressors. The blue curves are the fitted isentropic efficiency curves for LP and HP compressors respectively. The decreased fitting performance can be due to the fact that the compression ratio (τ) as the single variable is not enough to estimate isentropic efficiency for LP and HP compressors (Yang et al., 2009; Guth and Atakan, 2023; Tu and Chen, 2013). Therefore, isentropic efficiency fitted with multiple variables is proposed in this study.

$$\eta_{i,LP,\tau} = 0.6568 + 0.0194 \times \tau_{LP} - 0.0071 \times \tau_{LP}^2 \quad (10)$$

$$\eta_{i,HP,\tau} = 0.4262 + 0.1358 \times \tau_{HP} - 0.0198 \times \tau_{HP}^2 \quad (11)$$

The AHRI third-degree polynomials (AHRI 2020), which mainly describes the compressor mass flow rate and energy consumption based on the 10 coefficients depending on evaporating and condensing

Table 1
Unavailable variable inference methods tested in the model development.

Methods	Condenser outlet temperature		MT evaporators' Evaporating temperature		Isentropic efficiency	
Model	Scheme (a)	Scheme (b)	Constant	Variable	Single variable fitted	Multiple variables fitted
M1	✓		✓		✓	
M2	✓		✓			✓
M3	✓			✓	✓	
M4	✓			✓		✓
M5		✓	✓		✓	
M6		✓	✓			✓
M7		✓		✓	✓	
M8		✓		✓		✓

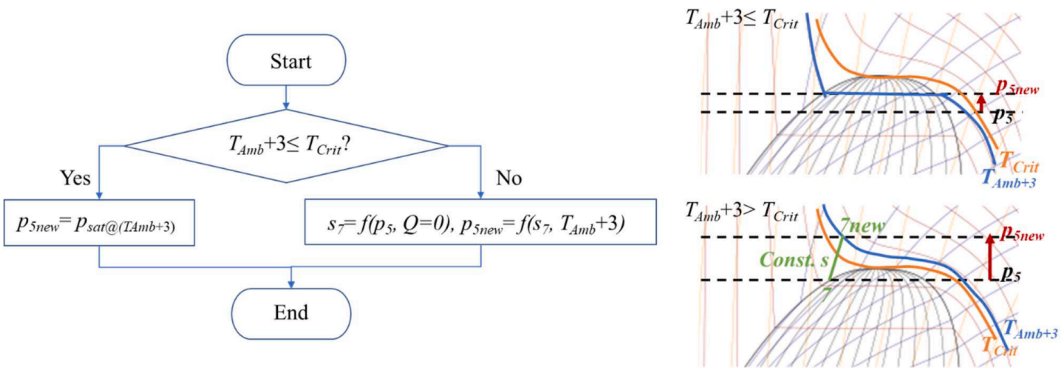

Fig. 3. The scheme (b) on condenser outlet temperature under the subcritical mode (left) and its representation in the pressure-enthalpy diagram (right).

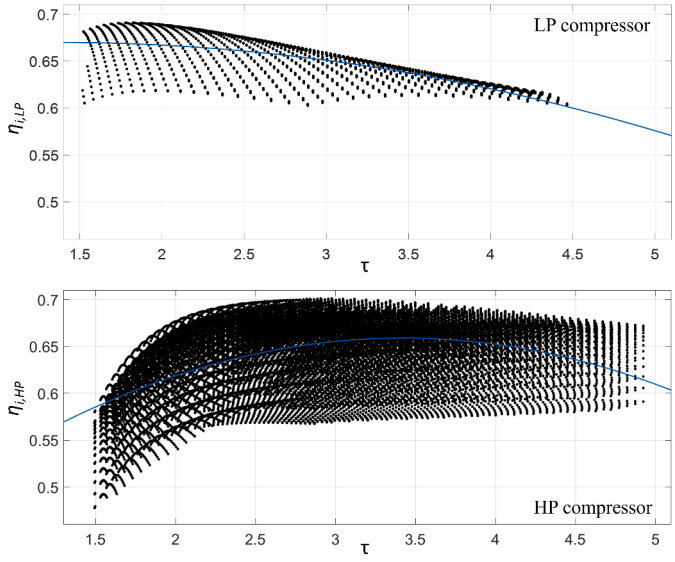

Fig. 4. The manufacturer data and the fitted curves for LP and HP compressors using the conventional method.

temperatures, are widely adopted in industry. Marchante-Avellaneda et al. (2023) suggested using condensation and evaporation pressure terms instead of the classical temperature domain and argued that the third-degree polynomials may cause overfitting problems. By referring to this concept and considering the available data from field measurements, our proposed method fits the isentropic efficiency for LP compressors ($\eta_{i,LP,multi}$) as a function of suction (P_1) and discharge (P_2) pressures of LP compressors (Liu et al., 2019), shown in Eq. (12). Since HP compressors can operate in both subcritical and transcritical mode and some of the HP compressors are VSD controlled, the isentropic efficiency for HP compressors under subcritical or transcritical mode ($\eta_{i,HP,sub/trans,multi}$) is separately fitted (Gullo et al., 2016) as a function of suction (P_4) and discharge (P_5) pressures as well as the real-time capacities of individual HP (HP_i%) compressors, shown in Eq. (13). The manufacturer data of LP and HP compressors were split randomly into 80 % for the training dataset and 20 % for the testing dataset. The coefficients of Eqs. (12) and (13) are obtained with the training dataset using the "lsqcurvefit" function in MATLAB, as shown in Tables 2 and 3. Table 4 summarizes the accuracy of the fitted isentropic efficiency

Table 2
Coefficients for isentropic efficiency equation of LP compressors.

a1	a2	a3	a4	a5	a6
0.3656	0.0032	0.0168	8.012×10^{-4}	-4.517×10^{-4}	-8.570×10^{-4}

Table 3
Coefficients for isentropic efficiency equations of HP compressors.

	a1	a2	a3	a4	a5
Subcritical	0.1901	-0.0102	0.0124	0.7818	-2.5216×10^{-4}
Transcritical	0.5182	-0.0025	-2.0448×10^{-4}	0.7551	-7.0899×10^{-5}

	a6	a7	a8	a9	a10
Subcritical	-1.5284×10^{-4}	-0.5246	3.0952×10^{-4}	7.3651×10^{-4}	-2.6900×10^{-4}
Transcritical	-7.5481×10^{-6}	-0.5074	5.0012×10^{-5}	0.0024	-8.6252×10^{-4}

equations for LP and HP compressors both with the training and testing datasets. Indicators including the coefficient of determination (R^2) and the mean absolute error (MAE) show good fitting performance. Furthermore, the third-degree polynomial is also tested and indicators for assessing the fitting performance are listed in Table 4. Both second-degree and third-degree polynomials offer satisfactory fitting accuracy, between which the third-degree polynomial performs slightly better. However, the third-degree polynomial has significantly increased the model complexity that coefficients for isentropic efficiency equation of LP and HP compressors are increased from six and ten to ten and twenty respectively. After discussing with store owners and managers from the practical perspective, the second-degree polynomial is more manageable and applicable thus is preferred. The isentropic efficiency of a multi-compressor pack is the weighted average of the isentropic efficiency of individual compressors concerning their real-time capacities.

$$\eta_{i,LP,multi} = a1 + a2 \times P_1 + a3 \times P_2 + a4 \times P_1 \times P_2 + a5 \times P_1^2 + a6 \times P_2^2 \tag{12}$$

$$\eta_{i,HP,sub/trans,multi} = a1 + a2 \times P_4 + a3 \times P_5 + a4 \times HP_i\% + a5 \times P_4^2 + a6 \times P_5^2 + a7 \times HP_i\%^2 + a8 \times P_4 \times P_5 + a9 \times P_4 \times HP_i\% + a10 \times P_5 \times HP_i\% \tag{13}$$

As a summary, there are both the conventional as well as the proposed inference methods for each of the above mentioned three unavailable variables, i.e. condenser outlet temperature, medium temperature (MT) evaporators' evaporating temperature and compressor isentropic efficiency. Specifically, *Scheme (a)* in condenser outlet temperature, *Constant* MT evaporators' evaporating temperature and *Single variable fitted* isentropic efficiency are the conventional methods; *Scheme (b)* in condenser outlet temperature, *Variable* MT evaporators' evaporating temperature and *Multiple variable fitted* isentropic efficiency are the proposed methods, as listed in Table 1. For the compressor mass flow rate, as another unavailable variable, only the proposed inference method is introduced in the next section. Therefore,

Table 4
Accuracy of the fitted isentropic efficiency equations for LP and HP compressors.

Polynomial	Index	LP compressors		HP compressors			
				Subcritical		Transcritical	
		Train (80 %)	Test (20 %)	Train (80 %)	Test (20 %)	Train (80 %)	Test (20 %)
Second degree	R^2	0.9597	0.9619	0.9827	0.9827	0.9738	0.9732
	MAE	0.0036	0.0036	0.0047	0.0048	0.0041	0.0041
Third degree	R^2	0.9945	0.9948	0.9994	0.9994	0.9995	0.9995
	MAE	0.0013	0.0013	0.0008	0.0008	0.0006	0.006

there are a total of eight models (M1-M8) with combinations of two inference methods for each of the three unavailable variables.

2.4.4. Compressor mass flow rate

Methods to obtain the compressor mass flow rates in previous works were omitted or mentioned vaguely. Therefore, an inference method is proposed in this study to estimate the refrigerant mass flow rates of LP and HP compressors (m_{LP} and m_{HP}) by considering the compressor performance curve and refrigeration cycle simultaneously. Specifically, the compressor performance curves regarding m_{LP} and m_{HP} are fitted using compressor manufacturer data based on a particular operating condition, which is defined by certain suction pressure, discharge pressure, superheat at the compressor inlet and the real-time compressor capacity. For LP compressors, their suction pressure (P_1), discharge pressure (P_2), superheat at compressor inlet ($SH_{LP} = T_1$-T_{15}) and the real-time compressor capacity (LP_i%) are all available from field measurements, as explained in Section 2.3. Thus m_{LP} can be directly estimated. However, since HP compressors lack the data of superheat at the compressor inlet (SH_{HP}), more information is needed for estimating m_{HP}. Here, the thermal balance and mass balance of CO_2 booster refrigeration systems are considered simultaneously to get another curve regarding m_{HP} as a function of superheat at compressor inlets. The intersection of these two curves means that an HP compressor operates at a particular operating condition in the CO_2 booster refrigeration systems, thus the corresponding mass flow rates are regarded as m_{HP}. Fig. 5 shows the schematic of m_{HP} inference method. More details are illustrated as follows.

After the preliminary analysis, the refrigerant mass flow rates of LP and HP compressors (m_{LP} and m_{HP}) are functions of the real-time capacities of individual HP (HP_i%) and LP (LP_i%) compressors which are obtained from field measurements, as shown in Eqs. (14) and (15). Where, $R_{LP,i}$ is the ratio of the mass flow rate at a particular operating condition to the overall minimum mass flow rate of an LP compressor ($m_{LP,i,min}$). $R_{LP,i}$ is fitted as a function of suction (P_1) as well as discharge (P_2) pressures and the superheat (SH_{LP}) at the inlet of the LP compressor using the data from the compressor manufacturer (Bitzer), shown as Eq. (16) with the coefficients listed in Table 5. LP_i% is the real-time capacities of individual LP compressors, LP_i% = 0 for LP compressor off and LP_i% = 100 % for LP compressor on. $N_{HP,on/off}$ is the number of on/off controlled HP compressors. $R_{HP,i}$ is the ratio of the mass flow rate at a particular operating condition to the overall minimum mass flow rate of a HP compressor ($m_{HP,i,min}$). It is fitted as a function of suction (P_4) as well as discharge (P_5) pressures and the superheat (SH_{HP}) at the inlet of the HP compressor using the data from the compressor manufacturer, shown in Eq. (17) with the coefficients listed in Table 5. $HP_{i,on/off}$% is the real-time capacities of individual on/off controlled HP compressors, $HP_{i,on/off}$% = 0 for HP compressor off and $HP_{i,on/off}$% = 100 % for HP compressor on. $N_{HP,VSD}$ is the number of VSD HP compressors. cf_i is the correction factor taking into account the impact of compressor part load operation on mass flow rate, which is fitted as a function of the real-time capacities of individual VSD HP compressors ($HP_{i,VSD}$%) with the data from the compressor manufacturer, shown as Eq. (18). It is worth noticing that $R_{LP,i}$ and $R_{HP,i}$ are dimensionless parameters which capture the fraction of the maximum mass flow rate at particular operating conditions and are applicable to various size compressors operating in the same pressure ranges. Given the data availability, m_{LP} can be directly calculated by Eq. (14), while m_{HP} needs to further consider the thermal balance and mass balance of CO_2 booster refrigeration systems as follows.

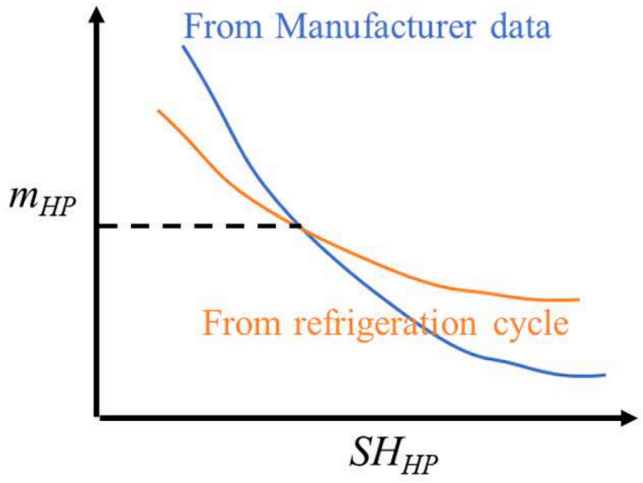

Fig. 5. Schematic of m_{HP} inference method.

$$m_{LP} = \sum_{i=1}^{N_{LP}} R_{LP,i} \times m_{LP,\ i,min} \times LP_i\% \tag{14}$$

$$m_{HP} = \sum_{i=1}^{N_{HP,on/off}} R_{HP,i} \times m_{HP,\ i,\ min} \times HP_{i,on/off}\% + \sum_{i=1}^{N_{HP,VSD}} R_{HP,i} \times m_{HP,\ i,\ min} \times cf_i \tag{15}$$

$$R_{LP,\ i} = b1 + b2\ \times P_1 + b3\ \times P_2 + b4\ \times SH_{LP} + b5\ \times P_1^2 + b6\ \times P_1 \times P_2 + b7\ \times P_1 \times SH_{LP} + b8\ \times P_2^2 + b9\ \times P_2 \times SH_{LP} + b10\ \times SH_{LP}^2 \tag{16}$$

$$R_{HP,\ i} = b1 + b2\ \times P_4 + b3\ \times P_5 + b4\ \times SH_{HP} + b5\ \times P_4^2 + b6\ \times P_4 \times P_5 + b7\ \times P_4 \times SH_{HP} + b8\ \times P_5^2 + b9\ \times P_5 \times SH_{HP} + b10\ \times SH_{HP}^2 \tag{17}$$

Table 5
Coefficients of the fitted equations for $R_{LP,i}$ and $R_{HP,i}$ (Eqs. (16) and (17)).

	b1	b2	b3	b4	b5
$R_{LP,i}$	-0.0767	0.2820	-0.0188	-0.0029	0.0011
$R_{HP,i}$	0.0370	0.1800	-0.0137	-0.0030	0.0012
	b6	b7	b8	b9	b10
$R_{LP,i}$	-0.0012	-0.0016	0.0001	0.0001	0.0001
$R_{HP,i}$	-0.0004	-0.0021	5.0921×10^{-5}	0.0002	0.0006

$$cf_i = 1.1061 HP_{i,VSD}\% - 0.1076 \quad (18)$$

m_{HP} is a function of superheat at compressor inlets when calculated using Eqs. (1)–(9) which describe the thermodynamic cycle of CO_2 booster refrigeration systems. According to the manufacturer documents, the recommended superheat temperature ranges between 10 °C and 40 °C. The superheat temperature below 10 °C can cause liquid slugging while the superheat temperature above 40 °C can cause insufficient motor cooling. A MATLAB function "fminbnd" is used to find a superheat temperature (between 10 °C and 40 °C) which minimizes the difference of HP compressor mass flow rate calculated by the compressor performance curve and refrigeration cycle. The corresponding compressor mass flow rate calculated by the compressor performance curve (Eqs. (14)–(18)) is regarded as actual m_{HP}.

3. Demonstration of the proposed modeling approach

The proposed modeling approach is implemented in three typical UK supermarket stores A-C. This section describes the implementation details in one of the stores (store A) which has the largest refrigeration cooling load. The other two stores B and C adopt a similar process and the results are discussed in Section 4.5.

3.1. Details of the tested supermarket store

The targeted supermarket store is located in south-central England. Two nearly identical CO_2 booster refrigeration systems (S1 and S2), shown in Fig. 1, are installed in this store. In each system, there are four HP compressors of the same product model, of which one is variable speed drive (VSD) controlled while others are with on/off control, and three LP compressors of the same product model, all of which are on/off controlled. For the gas coolers/condensers in both systems, the rated heat rejection rate is 412 kW and the fan power under the designed condition is 7 kW. The number of MT evaporators (e.g. display cabinets) and LT evaporators (e.g. cold rooms) in these two systems are approximately the same. The nominal total cooling capacity for MT evaporators in S1 and S2 are 180.9 kW and 185.7 kW respectively, and that for LT evaporators are 40.1 kW and 39.5 kW respectively.

Various meters (e.g. energy meters) and sensors (e.g. temperature sensors) are labeled by S1 and S2 depending on which CO_2 booster refrigeration systems they are installed in Their measurements are accessed from Building Management System (BMS). Normally available variables needed in model development from field measurements as mentioned in Section 2.3 can also be obtained from the online platforms of the target store. Specifically, discharge pressure of HP (P_5) and LP compressors (P_2), the real-time capacities of individual HP (HP_i%) and LP (LP_i%) compressors, and the ambient temperature (T_{Amb}) are sampled every 1 or 2 s. The whole year datasets from August 17th 2021 to August 17th 2022 are downloaded for model development. Besides these variables changing with the real-time operation of systems, there are variables to be regarded as constant across the year. The flash tank pressure ($P_8 = P_9 = P_{10}$) is 3.8×10^6 pa. The suction gas superheat (T_{14}-$T_{13} = T_1$-T_{16}) is 5 °C. The useful superheat (T_{13}-$T_{12} = T_{16}$-T_{15}) is 8 °C. The suction line pressure drop is the equivalent of 2 °C decrease in saturation temperature.

The electricity consumption, including compressors and gas cooler fans, of individual CO_2 booster refrigeration systems is measured hourly in the target store. The whole year datasets from August 17th 2021 to August 17th 2022 are downloaded and compared with the model output for model validation. More details can be found in Section 3.3.

3.2. Data processing and curation

The measured data from meters and sensors are not always high-quality. Data should be processed and then applied for model development to ensure satisfactory model performance (Xiao et al., 2022). Anomalous data causing integrity issues are identified. The operation conditions with incomplete and outlier data were deleted.

3.2.1. Condenser outlet temperature

The designed condenser/gas cooler approach temperature (min(T_7-T_{Amb})) is 3 °C. CO_2 refrigeration systems in the target store currently operate in floating condensing control (Ge and Tassou, 2014) where the discharge pressure of HP compressors (P_5) follows the ambient temperature (T_{Amb}) with no sub-cooling and 3 °C approach temperature between the condenser outlet temperature (T_7) and T_{Amb} in subcritical mode. Some abnormal circumstances affecting heat transfer or even breaking the thermodynamic laws regarding the designed approach temperature were identified during the data processing. 1.65 % and 3.65 % of measurements in S1 and S2 were with the temperature difference between T_7 and T_{Amb} to be less than the approach temperature (3 °C). 0.05 % and 0.06 % of measurements in S1 and S2 were with the smaller T_7 than T_{Amb}. This verifies the necessity of our proposed method for estimating condenser outlet temperature.

3.2.2. Evaporating temperature in MT evaporators

In this targeted store, the evaporating temperature in MT and LT evaporators are -9 °C and -34 °C in S1 and -7 °C and -34 °C in S2 by checking the design documents. Table 6 shows the distribution of calculated evaporating temperature in MT evaporators of two refrigeration systems (S1 and S2). The evaporating temperature in MT evaporators varied across the year. In S1, the median value was -6.67 °C and more than 95 % of samples were higher than -9 °C. In S2, the median value was -6.67 °C and more than 50 % of samples were higher than -7 °C. It conforms to the reality that open display cabinets (MT evaporators) are installed at the store and the evaporating temperature is not easy to be kept at the specified value (-9 °C and -7 °C) because of the disturbance from customer shopping behaviors and shopping area thermal environment maintained by HVAC systems. This verifies the necessity of our proposed method for estimating evaporating temperature in MT evaporators.

3.2.3. Processing of other variables for the model development

- Delete the stop operating conditions with either HP or LP compressors. They were mainly detected during the 2022 UK heatwave with record-breaking temperatures which led to a breakdown of refrigeration systems (Shah, 2022).
- Delete the outlier operation conditions with extreme discharge pressure of HP (P_5) and LP (P_2) compressors. Table 7 shows the distribution of measured discharge pressure of HP (P_5) and LP (P_2) compressors for the two refrigeration systems (S1 and S2) at the targeted store. After the preliminary analysis, the transcritical mode of the CO_2 booster refrigeration system accounts for a small portion. For example, 2.02 % of measurements in the first refrigeration system (S1) were in the transcritical mode. Therefore, with the increasing order, discharge pressure lower than 0.1 % and higher than 99.9 % of measurements (shaded area in Table 1) were regarded as extreme discharge pressure and removed from the dataset.

3.3. Test and validation of the proposed modeling approach

The proposed modeling method, including equations describing the thermodynamic cycle of CO_2 booster refrigeration systems, available variables by fully utilizing field measurements and unavailable variables inferred by different methods, is implemented in MATLAB and the refrigerant properties are calculated using the CoolProp (Bell et al., 2014). Specifically, model inputs, including the discharge pressure of HP (P_5) and LP compressors (P_2), the real-time capacities of individual HP (HP%) and LP (LP%) compressors and the ambient temperature (T_{Amb}), and the model output, i.e. the total electric power of individual CO_2 booster refrigeration systems ($W_{Tot,Cal}$), are measurements from BMS of

Table 6
Distribution of calculated evaporating temperature in MT evaporators ($T_{12,cal}$, °C) of two refrigeration systems (S1 and S2).

Distribution	min	1 %	5 %	25 %	50 %	75 %	95 %	99 %	max
S1	-17.68	-9.75	-8.80	-7.59	-6.67	-5.65	-4.54	-3.69	13.05
S2	-12.59	-10.71	-9.60	-7.85	-6.67	-5.65	-4.54	-3.93	2.27

Table 7
Distribution of measured discharge pressure of HP (P_5) and LP (P_2) compressors for the two refrigeration systems (S1 and S2) at the targeted store.

Refrigeration system	S1		S2	
Distribution	P_5 (Bar)	P_2 (Bar)	P_5 (Bar)	P_2 (Bar)
min	42.20	19.89	0	0
0.1 %	44.39	23.50	44.28	22.60
1 %	45.39	25.19	45.39	23.80
5 %	47.10	25.89	47.10	25.00
10 %	48.10	26.30	48.00	25.60
25 %	50.39	26.80	51.00	26.60
50 %	55.20	27.50	55.89	27.50
75 %	61.28	28.30	61.20	28.30
95 %	69.20	29.19	70.70	29.30
99 %	78.50	29.89	80.59	30.60
99.9 %	92.29	30.60	92.09	49.20
max	102.9	46.20	99.79	51.70

the target store. Variables which are unavailable but critical in model development include condenser outlet temperature, medium temperature (MT) evaporators' evaporating temperature and compressor isentropic efficiency. They can either be inferred by proposed and conventional methods, as detailed in Section 2.4 and summarized in Table 1. As for the compressor mass flow rate, only the proposed one is programmed. In summary, eight models with different combinations are developed to test the proposed modeling approach with the proposed inference methods for unavailable variables. The flowchart of model development and implementation is shown in Fig. 6.

The models are validated by comparing the actual electricity consumption of the CO_2 booster refrigeration systems in the targeted store and the consumption predicted by the model. The outputs calculated by the model for each sampled timestamp are averaged hourly to compare with measured hourly electricity consumption data. Since there are two nearly identical CO_2 booster refrigeration systems (S1 and S2) in the target store, the model implementation and validation processes are repeated for each of them. After the data processing and curation, as explained in Section 3.2, there are more than 8700 hourly samples for both S1 and S2 in the whole year datasets (from August 17th 2021 to August 17th 2022). As an example, Fig. 7 shows the M8 modeled and measured power consumption for a summer week (left) and a winter week (right) of two CO_2 booster refrigeration systems (S1 and S2) in the target store. M8 reproduces actual behaviors of the refrigeration systems in a good way.

To better validate the proposed modeling approach by comparing with conventional modeling approaches, four performance indicators, i.e. average error, standard deviation of error, annual energy error and R^2, are adopted and the model validation results of S1 and S2 in the store are summarized in Tables 8 and 9. The average error and the standard deviation of error are the average and the standard deviation of the hourly relative error of the modelled electricity consumption with respect to the actual electricity consumption. The annual energy error is the annual relative error of the modelled with respect to the actual electricity consumption. It is difficult to justify which indicator is more important. For example, there is a drawback of annual energy error as the most important indicator that there are samples with high positive deviations and low negative deviations. When calculating the annual energy error, all samples are summed up as the modelled annual electricity consumption and compared with the actual annual electricity consumption, thus those positive and negative deviations cancel with each other and a very small annual energy error is obtained. Standard deviation of error helps to identify this situation. Therefore, the four performance indicators listed in Tables 8 and 9 were considered simultaneously as a

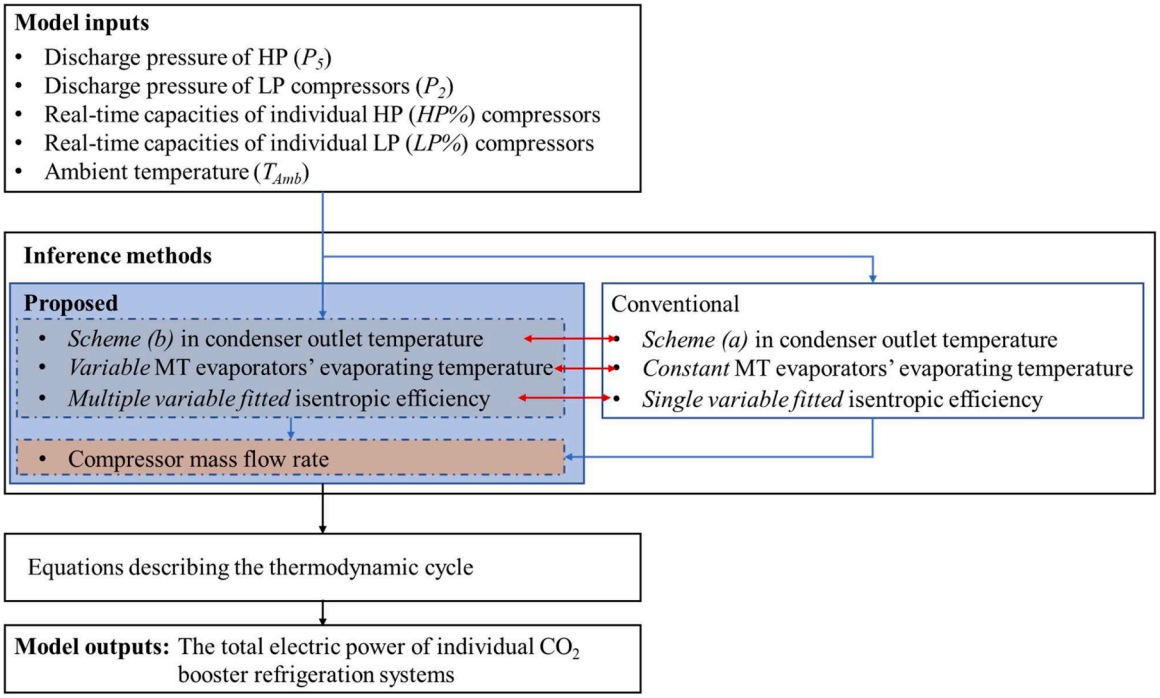

Fig. 6. The flowchart of model development and implementation.

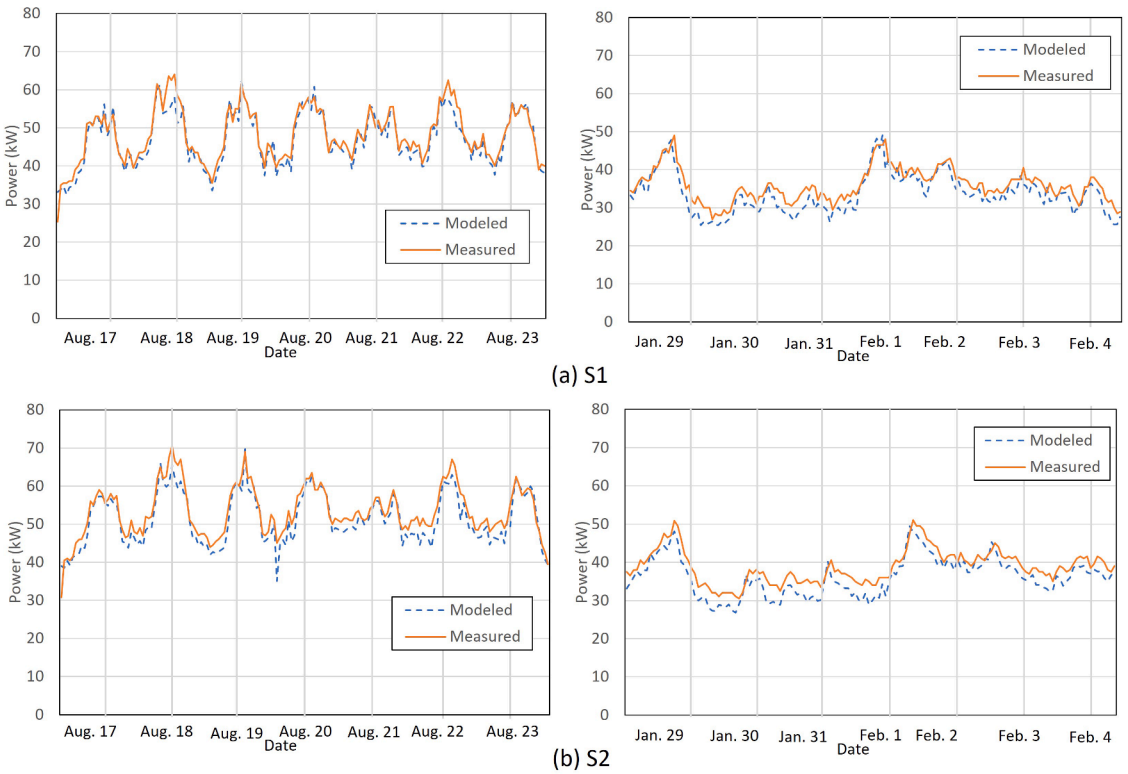

Fig. 7. M8 modeled and measured power consumption for a summer week (left) and a winter week (right) of two CO_2 booster refrigeration systems (S1 and S2) in the target store.

Table 8
Model validation results for the first CO_2 booster refrigeration systems (S1).

Model	Average error (%)	Standard deviation of error (%)	Annual energy error (%)	Coefficient of determination (R^2)
M1	4.70	5.80	0.54	0.96
M2	7.08	5.64	5.90	0.92
M3	4.95	6.10	0.72	0.96
M4	4.09	3.80	2.10	0.97
M5	4.70	5.79	0.55	0.96
M6	7.08	5.64	5.91	0.92
M7	4.95	6.09	0.72	0.96
M8	**4.09**	**3.80**	**2.11**	**0.97**

Table 9
Model validation results for the second CO_2 booster refrigeration systems (S2).

Model	Average error (%)	Standard deviation of error (%)	Annual energy error (%)	Coefficient of determination (R^2)
M1	4.12	7.17	0.01	0.96
M2	6.65	6.65	5.84	0.91
M3	4.39	7.50	1.37	0.95
M4	2.49	6.79	2.10	0.96
M5	4.12	7.17	0.05	0.96
M6	6.65	6.65	5.85	0.91
M7	4.39	7.49	1.37	0.95
M8	**2.51**	**6.78**	**2.13**	**0.96**

whole.

For both systems (S1 and S2), the 8th model (M8) with all proposed methods, i.e. *Scheme (b)* in condenser outlet temperature, *Variable* MT evaporators' evaporating temperature and *Multiple variable fitted* isentropic efficiency, performed the best. The bolded parts in Tables 8 and 9 show their very low average error, standard deviation of error, annual energy error and very high R^2 compared to other models with inferences all or partly made by the conventional methods. The 1st model (M1) with all estimations made by the conventional methods, i.e. *Scheme (a)* in condenser outlet temperature, *Constant* MT evaporators' evaporating temperature and *Single variable fitted* isentropic efficiency, performed the worst. By adopting the proposed inference methods in S1 and S2 separately, the average error decreased from 4.7 % to 4.09 % and 7.17 % to 6.78 %, the standard deviation of error decreased from 5.80 % to 3.80 % and 24.83 % to 10.16 %, the annual energy error increased from 0.54 % to 2.11 % and 0.01 % to 2.13 % but still very small, and R^2 increased from 0.96 to 0.97 in S1 and kept as 0.96 unchanged in S2.

The superiority of the proposed model approach with all proposed inference methods results from its ability to fully utilise the available field measurements, ensure data integrity and avoid breaking thermodynamic laws, which can be highlighted by discussing the effects of individual proposed inference methods in Section 4.

4. Discussions

Effects on the model performance by using the proposed methods to estimate individual variables, i.e. *Scheme (b)* in condenser outlet temperature, *Variable* MT evaporators' evaporating temperature, *Multiple variable fitted* isentropic efficiency and compressor mass flow rate, are discussed in Sections 4.1–4.4. The model performance in the other two stores using the proposed modeling approach is explained in Section 4.5.

4.1. Effects of condenser outlet temperature

Effects of condenser outlet temperature estimated by the proposed methods, i.e. scheme (b), are tested by comparing models 1 and 5, 2 and 6, 3 and 7, as well as 4 and 8 for each of the systems. Tables 8 and 9 show that most of the indicators did not change. Meanwhile, for those with slightly improved indicators (e.g. standard deviation of error was decreased from 5.80 % to 5.79 % by comparing models 1 and 5 in S1)

and slightly deteriorated indicators (e.g. annual energy error was increased from 5.90 % to 5.91 % by comparing models 2 and 6 in S1), the performance difference was also so small to be negligible. However, it is not conclusive that effects of condenser outlet temperature on model performance are insignificant, because the abnormal data regarding approach temperature took up a small part of the whole dataset (1.70 % in S1 and 3.71 % in S2 by the data processing in Section 3.2.1). It is very likely that the model performance difference would be more evident if the dataset quality was lower and the abnormal data amount regarding approach temperature was larger. Moreover, *Scheme (b)* in condenser outlet temperature is proposed to ensure thermodynamic laws and data integrity regarding the approach temperature rather than purely match the model output with the electricity consumption of CO_2 refrigeration systems measured by their data collection systems. This is of vital importance when the developed model is applied for testing other operation settings, in which actual electricity consumption data is unavailable and operating parameters need to be adjusted without breaking thermodynamic laws, before really adopting them in actual operation. A good example is to test different heat recovery strategies by adjusting the operating parameters (e.g. discharge pressure of HP compressors) for different amounts of recoverable heat.

4.2. Effects of MT evaporators' evaporating temperature

Effects of the estimation on MT evaporators' evaporating temperature made by the proposed methods, i.e. variable MT evaporators' evaporating temperature, are tested by comparing models 1 and 3, 2 and 4, 5 and 7, as well as 6 and 8 for each of the systems. Compared to the effects of condenser outlet temperature, the effects of MT evaporators' evaporating temperature are more evident. Tables 8 and 9 show that the model performance was improved by comparing models 2 and 4 as well as 6 and 8 in both S1 and S2. However, the model performance was deteriorated by comparing models 1 and 3 as well as 5 and 7 in both S1 and S2. These opposite results are because the compressor isentropic efficiency was calculated using either multiple variables fitted or single variable fitted equations.

The proposed inference method fully utilizes the available measured data, i.e. discharge pressure of LP compressors (P_2), which has the following two aspects of effects. On the one hand, the mass flow rates of LP and HP compressors are better estimated as mentioned in Section 2.4.4. On the other hand, isentropic efficiency for LP and HP compressors are functions of P_2 both using single variable fitted equations (Eqs. (11) and (12)) and multiple variables fitted equations (Eqs. (13) and (14)) as mentioned in Section 2.4.3. Fig. 8 shows the isentropic efficiency of LP and HP compressors of models 6 and 8 (M6 and M8) in S1, i.e. both using multiple variables fitted equations. When adopting constant MT evaporators' evaporating temperature in S1 (M6), the isentropic efficiency of both LP and HP compressors is distributed in a narrower range. Particularly, there was only one value for the isentropic efficiency of LP compressors since suction (P_1) and discharge (P_2) pressures were both constants using the conventional inference method. The conventional inference method fails to reflect the actual isentropic efficiency of compressors, which explains the opposite effects of MT evaporators' evaporating temperature on model performance.

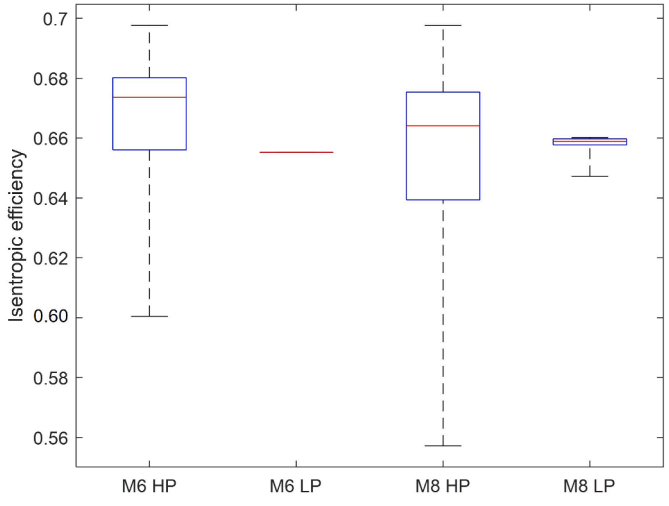

Fig. 8. Isentropic efficiency of LP and HP compressors of models 6 and 8 (M6 and M8) in S1.

4.3. Effects of isentropic efficiency

Effects of the estimation on isentropic efficiency made by the proposed method, i.e. multiple variables fitted equations, are tested by comparing models 1 and 2, 3 and 4, 5 and 6, as well as 7 and 8 for each of the systems. The effects of isentropic efficiency are also evident. Tables 8 and 9 show that the model performance was improved by comparing models 3 and 4 as well as 7 and 8 in both S1 and S2. However, the model performance deteriorated by comparing models 1 and 2 as well as 5 and 6 in both S1 and S2. These opposite results are because the MT evaporators' evaporating temperature was calculated either as variables or as a constant. The reasons for these opposite effects are explained in Section 4.2. In summary, although multiple variables fitted equations better reflect the actual compressor characteristics, the calculated isentropic efficiency is very sensitive to the inputs. Inputs with better quality (variable MT evaporators' evaporating temperature) improve the model performance, while inputs with worse quality (constant MT evaporators' evaporating temperature) deteriorate the model performance. Therefore, it is suggested that if there is available discharge pressure of LP compressors, it should be utilized fully such as to estimate MT evaporators' evaporating temperature and multiple variables fitted isentropic efficiency will be used. Otherwise, it is suggested to choose a single-variable fitted isentropic efficiency.

4.4. Effects of compressor mass flow rate

Table 10 shows the distribution of the HP compressor mass flow rate difference calculated by the compressor performance curve and refrigeration cycle (mentioned in Section 2.4.4) of two CO_2 booster refrigeration systems (S1 and S2). In the first CO_2 booster refrigeration system (S1), the median value was 9.24×10^{-4} kg/h and more than 95 % of samples were smaller than 4.32×10^{-3} kg/h. In the second CO_2 booster refrigeration system (S2), the median value was 7.78×10^{-4} kg/h and more than 95 % of samples were smaller than 4.94×10^{-3} kg/h. Thus, the HP compressor mass flow rate differences of most of the samples were very small, and particular operating conditions of HP compressors operating in two CO_2 booster refrigeration systems were well identified. The corresponding HP compressor mass flow rate can be regarded as m_{HP}. The proposed method for compressor mass flow rate estimation works well in model development. However, there were few samples with large HP compressor mass flow rate differences (e.g. the maximum value were 2382.17 and 3198.11 in S1 and S2 respectively). There are two possible reasons for being unable to find proper values in these cases. First is because the superheat temperature at the inlet of HP

Table 10
Distribution of the HP compressor mass flow rate difference of two CO_2 booster refrigeration systems (S1 and S2).

Distribution	min	5 %	25 %	50 %	75 %	95 %	max
S1 (kg/h)	1.85×10^{-8}	7.62×10^{-5}	4.13×10^{-4}	9.24×10^{-4}	2.01×10^{-3}	4.32×10^{-3}	2382.17
S2 (kg/h)	1.44×10^{-9}	6.47×10^{-5}	3.50×10^{-4}	7.78×10^{-4}	2.07×10^{-3}	4.94×10^{-3}	3198.11

compressors was out of the range between 10 °C and 40 °C. HP compressors operated in abnormal conditions with liquid slugging and insufficient motor cooling, for which the manager of the store would be notified by an alarm. The second is because of the wrongly measured data. Mitigation measures by slightly modifying the discharge pressure of HP compressors (P_5) or the capacities of VSD HP compressors are proposed accordingly which solve those abnormal operating conditions.

4.5. Model generalization evaluated in additional two stores

The proposed modeling approach is implemented in three typical UK supermarket stores A-C of different sizes. Store B is located in east England and store C is located in southwest England. They have different refrigeration cooling loads, of which are from store A to store C in descending order. There are two nearly identical CO_2 booster refrigeration systems (S1 and S2) in each of the stores. Compared to the one VSD-controlled and three on/off-controlled HP compressors at store A, there are one VSD-controlled and two on/off-controlled HP compressors at stores B and C. There are three on/off-controlled LP compressors at all three stores. Different product models for compressors and condensers/gas coolers are used in each store. A demonstration of the proposed modeling approach in store A is illustrated in Section 3. Following a similar process, the proposed modeling approach is tested and validated using high-resolution measurements across the whole year from the other two stores B and C. As discussed in previous sections, the proposed modeling approach with the proposed inference methods for missing variables, i.e. *Scheme (b)* in condenser outlet temperature, *Variable* MT evaporators' evaporating temperature and *Multiple variable fitted* isentropic efficiency, performs the best. Thus, Fig. 9 shows the performance of the proposed modeling approach, evaluated by average error, standard deviation of error, annual energy error and R^2, in stores B and C. In store B, average error were 5.43 % and 5.20 %, standard deviation of error were 8.02 % and 6.50 %, annual energy error were 2.20 % and 2.29 %, R^2 were 0.94 and 0.93 in S1 and S2 respectively. In store C, only S2 had useable field measurements and average error, standard deviation of error, annual energy error and R^2 were 5.20 %, 9.68 %, 2.07 % and 0.90 respectively. These high values highlight the satisfactory performance of the proposed modeling approach when generalized to different stores.

The model inputs are essential for the high-fidelity model proposed in this work, which means at the current stage the proposed model cannot be generalized to other standard CO_2 booster refrigeration systems without any on-site measurements/data. However, the inputs adopted in this work are normally available from field measurements of real cases, thus no extra effort is needed for data collection and the high-fidelity model is able to be reused in other cases. The number of model inputs can be further reduced by some simplification methods with the risk of deteriorating model performance. For example, since the CO_2 systems are operated in floating control mode, the discharge pressure of HP (P_5) can be fitted as a function of ambient temperature (T_{Amb}) and the number of model inputs is reduced from five to four. Similar ideas for other inputs while keeping the satisfactory model performance will be explored in the follow-up research.

5. Conclusions

A steady-state theoretical model for CO_2 booster refrigeration systems is developed and validated against field measurements from three UK supermarkets. The available measurements are utilized to the best level to ensure model accuracy and physical interpretability. Methods to infer the missing information in CO_2 refrigeration systems are proposed. Variables which are normally unavailable in field measurements but critical in model development are considered, i.e. condenser outlet temperature, evaporating temperature, compressor isentropic efficiency and compressor mass flow rate. Based on the experiences and results of the test case, conclusions can be summarized as follows:

- By implementing the proposed modeling approach using the high-resolution field measurements across the whole year from the CO_2 booster refrigeration systems in three real UK supermarkets, the proposed modeling approach is validated to improve the model performance effectively compared to conventional modeling approaches. The model (M8) developed using the proposed model approach had a small average error, standard deviation of error, annual energy error and large R^2. For instance in S1 of store A, the

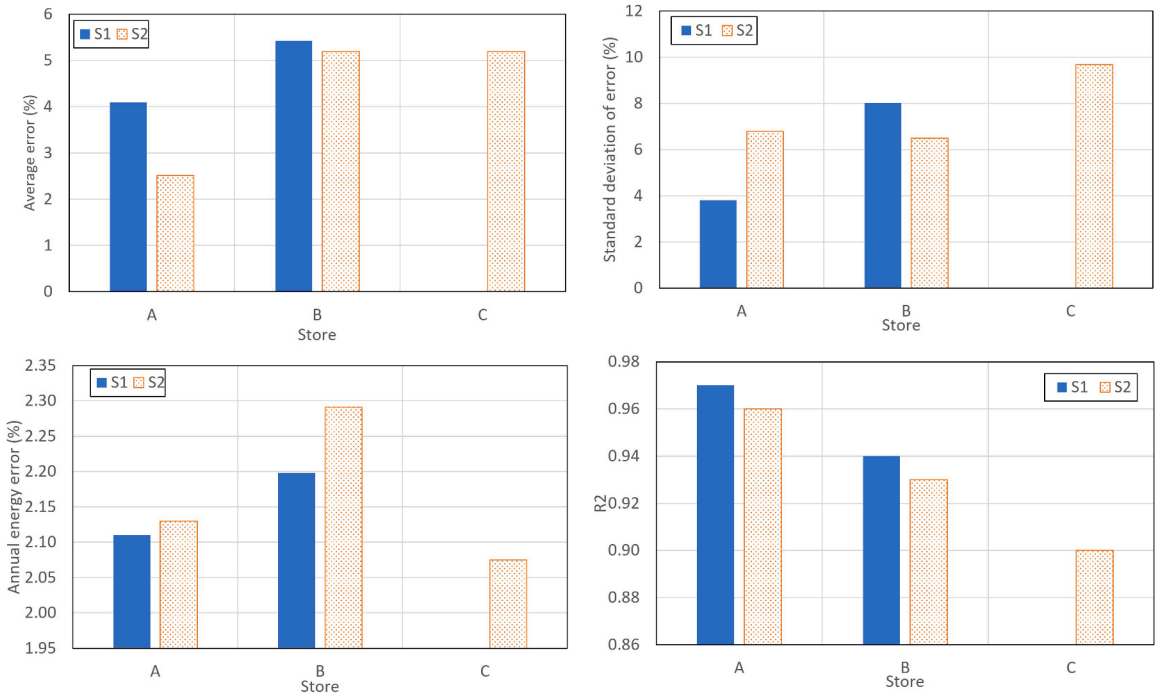

Fig. 9. Model performance in all three tested stores A-C.

average error was 4.09 %, the standard deviation of error was 3.80 %, the annual energy error was 2.11 % and the R^2 was 0.97.

- The proposed inference method for condenser outlet temperature enhances the abilities of the proposed model approach to ensure data integrity and avoid breaking thermodynamic laws. This is of vital importance when the developed model is applied for testing other operation settings before really adopting them in actual operation. A good example is to test different heat recovery strategies for different amounts of recoverable heat by adjusting the operating parameters (e.g. discharge pressure of HP compressors) while making sure the operating conditions are thermodynamically possible.
- The proposed inference methods on evaporating temperature and isentropic efficiency intercorrelate with each other, and they improve the accuracy of the proposed model approach altogether by reflecting the real-time actual values of missing variables rather than rough assumptions. Variable MT evaporators' evaporating temperature and multiple variables fitted isentropic efficiency, inference methods proposed in this study, provide the best model performance since they utilize the available field measurements to the best level.
- The compressor mass flow rate inference method is proposed by considering the compressor performance curve and refrigeration cycle simultaneously. It manages to supplement compressor mass flow rate, a critical variable but is seldom measured, for model development. It worked well for most of the working conditions (more than 95 % of samples) of CO_2 refrigeration systems. For a small part of the working conditions (<5 % of samples), it could be adopted as an anomaly detection method for liquid slugging and insufficient motor cooling of compressors in CO_2 refrigeration systems and mitigated by minor modification of operating parameters.

CRediT authorship contribution statement

Wenzhuo Li: Writing – original draft, Methodology, Formal analysis, Data curation. **Ivan Korolija:** Writing – review & editing, Supervision, Methodology, Conceptualization. **Rui Tang:** Writing – review & editing, Supervision, Conceptualization, Funding acquisition, Methodology. **Dejan Mumovic:** Writing – review & editing, Supervision, Funding acquisition.

Declaration of interests

The authors declare that they have no known competing financial interests or personal relationships that could have appeared to influence the work reported in this paper.

Acknowledgments

This work was supported by the Knowledge Transfer Partnership (KTP) project of Innovate UK (number is KTP12913) and the UCL Knowledge Exchange and Innovation Funding.

References

Version E. 8.9. 0 Documentation Engineering Reference, 2018. US Department of Energy, pp. 362–367.
AHRI, 2020. Performance rating of positive displacement refrigerant compressors. AHRI Standard 540.
Azzolin, M., Cattelan, G., Dugaria, S., Minetto, S., Calabrese, L., Del Col, D., 2021. Integrated CO2 systems for supermarkets: field measurements and assessment for alternative solutions in hot climate. Appl. Therm. Eng. 187.
Bell, I.H., Wronski, J., Quoilin, S., Lemort, V., 2014. Pure and pseudo-pure fluid thermophysical property evaluation and the open-source thermophysical property library CoolProp. Ind. Eng. Chem. Res. 53, 2498–2508.
British Retail Consortium (BRC), 2024. Climate Action Roadmap. Net Zero Roadmap for the Retail Industry. Available online: https://brc.org.uk/climate-roadmap/. accessed on 24 August.
D'Agaro, P., Coppola, M.A., Cortella, G., 2019. Field tests, model validation and performance of a CO2 commercial refrigeration plant integrated with HVAC system. Int. J. Refrig. 100, 380–391.
Department for Business, 2024. Energy & Industry Strategy. Building Energy Efficiency Survey. Executive Summary. Available online: https://assets.publishing.service.gov.uk/media/5a8185ede5274a2e87dbe162/BEES_Executive_Summary_FINAL.pdf. accessed on 24 August.
European Commision. EU building stock observatory. Available online: https://energy.ec.europa.eu/topics/energy-efficiency/energy-efficient-buildings/eu-building-stock-observatory_en (accessed on 27 August 2024).
Ferreira, A., Pinheiro, M.D., de Brito, J., Mateus, R., 2019. Decarbonizing strategies of the retail sector following the Paris agreement. Energy Policy 135, 110999.
Ge, Y., Tassou, S., 2011. Performance evaluation and optimal design of supermarket refrigeration systems with supermarket model "SuperSim". Part II: model applications. Int. J. Refrig. 34, 540–549.
Ge, Y.T., Tassou, S.A., 2014. Control optimizations for heat recovery from CO2 refrigeration systems in supermarket. Energy Convers. Manag. 78, 245–252.
Giunta, F., Sawalha, S., 2021. Techno-economic analysis of heat recovery from supermarket's CO2 refrigeration systems to district heating networks. Appl. Therm. Eng. 193, 117000.
Granell, R., Axon, C.J., Kolokotroni, M., Wallom, D.C., 2021. Predicting electricity demand profiles of new supermarkets using machine learning. Energy Build. 234, 110635.
Gulliford, M.J., Orlebar, R.H., Bird, M.H., Acha, S., Shah, N., 2022. Developing a dynamic carbon benchmarking method for large building property estates. Energy Build. 256, 111683.
Gullo, P., Elmegaard, B., Cortella, G., 2016. Energy and environmental performance assessment of R744 booster supermarket refrigeration systems operating in warm climates. Int. J. Refrig. 64, 61–79.
Guth, T., Atakan, B., 2023. Semi-empirical model of a variable speed scroll compressor for R-290 with the focus on compressor efficiencies and transferability. Int. J. Refrig. 146, 483–499.
Hart, M., Austin, W., Acha, S., Le Brun, N., Markides, C.N., Shah, N, 2020. A roadmap investment strategy to reduce carbon intensive refrigerants in the food retail industry. J. Clean. Prod. 275, 123039.
Inderwildi, O., Zhang, C., Wang, X., Kraft, M., 2020. The impact of intelligent cyber-physical systems on the decarbonization of energy. Energy Environ. Sci. 13, 744–771.
Lagoeiro, H., Marques, A., Davies, G., Foster, A., Evans, J., Jans-Singh, M., Maidment, G., 2024. Quantifying energy consumption and carbon emissions from retail refrigeration in the UK. In: 2024 8th IIR International Conference on Sustainability and the Cold Chain: International Institute of Refrigeration.
Liang, X., Zhu, X., Chen, S., Jin, X., Xiao, F., Du, Z, 2023. Physics-constrained cooperative learning-based reference models for smart management of chillers considering extrapolation scenarios. Appl. Energy 349.
Liu, X., Fu, R., Wang, Z., Lin, L., Sun, Z., Li, X., 2019. Thermodynamic analysis of transcritical CO2 refrigeration cycle integrated with thermoelectric subcooler and ejector. Energy Convers. Manag. 188, 354–365.
Liu, Y., Liu, J., Yu, J., 2020. Theoretical analysis on a novel two-stage compression transcritical CO2 dual-evaporator refrigeration cycle with an ejector. Int. J. Refrig. 119, 268–275.
Maouris, G., Sarabia Escriva, E.J., Acha, S., Shah, N., Markides, C.N, 2020. CO2 refrigeration system heat recovery and thermal storage modelling for space heating provision in supermarkets: an integrated approach. Appl. Energy 264.
Marchante-Avellaneda, J., Corberan, J.M., Navarro-Peris, E., Shrestha, S.S., 2023. A critical analysis of the AHRI polynomials for scroll compressor characterization. Appl. Therm. Eng. 219.
Mota-Babiloni, A., Navarro-Esbrí, J., Barragán-Cervera, Á., Molés, F., Peris, B., Verdú, G., 2015. Commercial refrigeration–an overview of current status. Int. J. Refrig. 57, 186–196.
Mylona, Z., Kolokotroni, M., Tassou, S.A., 2017. Frozen food retail: measuring and modelling energy use and space environmental systems in an operational supermarket. Energy Build. 144, 129–143.
Paurine, A., Maidment, G., Rodway, M., Yebiyo, M., 2021. Understanding the market need for skills in alternative refrigerants with low global warming potential in the EU region–a comprehensive survey on Refrigerant Emissions And Leakage (REAL) alternatives programme. Int. J. Refrig. 122, 11–20.
Pérez-Segarra, C.D., Rigola, J., Sòria, M., Oliva, A., 2005. Detailed thermodynamic characterization of hermetic reciprocating compressors. Int. J. Refrig. 28, 579–593.
Polzot, A., 2017. Energy Benefit Assessment of Various Refrigeration Systems Integrated with HVAC Units in Shopping Malls. University of Udine.
Polzot, A., D'Agaro, P., Cortella, G, 2017. Energy analysis of a transcritical CO2 supermarket refrigeration system with heat recovery. Energy Procedia 111, 648–657.
Polzot, A., Gullo, P., D'Agaro, P., Cortella, G, 2016. Performance evaluation of a R744 booster system for supermarket refrigeration, heating and DHW. In: Proceedings of the 12th IIR Gustav Lorentzen Natural Working Fluids Conference. Edinburgh, UK, pp. 21–24.
Royal Institution of Chartered Surveyors (RICS). Energy efficiency of the building stock in the EU. 2020. Available online: https://www.rics.org/news-insights/energy-efficiency-of-the-building-stock-in-the-eu (accessed on 27 August 2024).
Sacasas, D., Vega, J., Cuevas, C., 2022. An annual energetic evaluation of booster and parallel refrigeration systems with R744 in food retail supermarkets. A Chilean perspective. Int. J. Refrig. 133, 326–336.
Salehy, Y., Hoang, H.M., Cluzel, F., Leroy, Y., Delahaye, A., Fournaison, L., Yannou, B., 2020. Energy performances assessment for sustainable design recommendations: case study of a supermarket's refrigeration system. Procedia CIRP. 90, 328–333.
Sarabia Escriva, E.J., Acha, S., Le Brun, N., Soto Francés, V., Pinazo Ojer, J.M., Markides, C.N., Shah, N, 2019. Modelling of a real CO2 booster installation and

evaluation of control strategies for heat recovery applications in supermarkets. Int. J. Refrig. 107, 288–300.
Sarabia Escriva, E.J., Hart, M., Acha, S., Soto Francés, V., Shah, N., Markides, C.N., 2022. Techno-economic evaluation of integrated energy systems for heat recovery applications in food retail buildings. Appl. Energy 305.
Sawalha, S., 2013. Investigation of heat recovery in CO2 trans-critical solution for supermarket refrigeration. Int. J. Refrig. 36, 145–156.
Shah, F., 2022. Supermarkets Forced to Empty Shelves as Heatwave Causes Chillers to Breakdown. The independent.
Skačanová K. F-Gas regulation shaking up the HVAC&R Industry. shecco; 2016.
Söylemez, E., Hafner, A., Schlemminger, C., Kriezi, E.E., Khorshidi, V., 2022. The performance analysis of an integrated CO2 refrigeration system with multi-ejectors installed in a Supermarket. Energies. 15, 3142.
Sun, Z., Li, J., Liang, Y., Sun, H., Liu, S., Yang, L., et al., 2020b. Performance assessment of CO2 supermarket refrigeration system in different climate zones of China. Energy Convers. Manag. 208.
Sun, Z., Li, J., Liang, Y., Sun, H., Liu, S., Yang, L., et al., 2020a. Performance assessment of CO2 supermarket refrigeration system in different climate zones of China. Energy Convers. Manag. 208.
The GreenChill Program, 2022. Keeping Cool For Fifteen Years 2007-2022. U.S. Environmental Protection Agency. Available online. https://www.epa.gov/system/files/documents/2022-09/GreenChill-Keeping-Cool-for-15-Years-2022_1.pdf. accessed on 15 October 2024.
Tsamos, K., Ge, Y., Santosa, I., Tassou, S., 2017. Experimental investigation of gas cooler/condenser designs and effects on a CO2 booster system. Appl. Energy 186, 470–479.
Tu, H., Chen, H., 2013. Modeling of a compressor's performance map by fitting function methodology. Adv. Mat. Res. 779, 1194–1198.
Xiao, Z., Gang, W., Yuan, J., Chen, Z., Li, J., Wang, X., Feng, X., 2022. Impacts of data preprocessing and selection on energy consumption prediction model of HVAC systems based on deep learning. Energy Build. 258, 111832.
Yang, L., Zhao, L.-X., Zhang, C.-L., Gu, B., 2009. Loss-efficiency model of single and variable-speed compressors using neural networks. Int. J. Refrig. 32, 1423–1432.